Available online at www.sciencedirect.com
SCIENCE DIRECT®
Journal of Sound and Vibration 273 (2004) 969–987
JOURNAL OF SOUND AND VIBRATION
www.elsevier.com/locate/jsvi

Scattering of plane wave from moving body underwater with finite impedance surface

T.Q. Wang*, Z.G. Yang

Department of Jet Propulsion, Beijing University of Aeronautics and Astronautics, Beijing 100083, People's Republic of China

Received 18 July 2001; accepted 29 April 2003

Abstract

An acoustic analogy model and numerical approach to predict propeller aircraft sound field have been developed to predict the scattering of incident plane wave by moving body with the surface of finite impedance. The scale rule of Mach number and Helmholtz number in the model was derived and demonstrated in the numerical experiments. Two types of check in numerical experiments illustrate the validity of the present model and the numerical approach developed in present paper. The effect of Helmholtz number and movement velocity has been discussed finally.

1. Introduction

This paper presents a method to predict the scattering of plane wave by moving objects with the surface of finite impedance that can be applied in the stealth design of underwater targets.

In order to investigate the echo information of underwater targets, the scattering of acoustic wave by objects in varying boundary condition has been studied in numerous references. The deformed cylinder method (DCM) of Stanton [1–3] uses the analytical solution to estimate the scattering response from any axisymmetric body or from spherical and elongated shelled bodies with high aspect ratio in variant boundary condition. It is an approximate method adapted to the specified body shape, and is limited to broadside incidence and back scattering only. The boundary element/finite element methods are the more versatile approaches to calculate the

*Corresponding author. Tel.: +86-10-823-17407; fax: +86-10-823-29401.
E-mail address: wangtq@buaa.edu.cn (T.Q. Wang).

0022-460X/03/$ - see front matter
doi:10.1016/S0022-460X(03)00515-7

scattering sound field or radiating sound field by an object submerged in fluid [4–6], but it is difficult to account for the target movement effects by these methods indeed. The boundary condition is crucial for acoustic scattering by a body and is determined by the body structure (rigid, solid elastic, a sell, coated or uncoated with layer of viscoelastic material, etc.) that causes different amount of the acoustic energy of incident wave to be absorbed and different scattering. In the rigid boundary or pressure release boundary no acoustic energy of incident wave is absorbed by the object, in some other type of boundary an amount of acoustic energy of incident wave is absorbed by the body or by the layer coated on the body surface. Based on the Lighthill's acoustic analogy Ffowcs Williams and Hawkings converted the moving boundary condition to the sources on the right side of the inhomogeneous wave equation named as FW–H equation [7] and the boundary sources include the monopolies induced by the surface displacement and the dipoles induced by the surface loads which have been successfully used to predict the propeller noise by Farassat [8]. By using Farassat's integral formulation to calculate the sound field of surface sources as well as the united aerodynamics and aeroacoustics approach given by Farassat and Long [9,10], Wang has developed a model to solve the coupling between the propeller sound sources and the rigid fuselage or elastic fuselage [11,12], further the model has been successfully used to calculate the radiating sound field by the vibrating surface moving at small Mach number [13], to calculate wing shielding effect of propeller aircraft [14] and to predict the underwater target strength of rigid body [15].

In the present paper the model has been developed to predict the scattering of plane wave by a body with the surface of finite impedance that is a representative boundary in practice and herewith is considered as local reacting surface or the surface similar to the interface between two fluids. The paper derives a math-physical model: a governing equation to calculate the total sound pressure on the surface and a formula to calculate the scattering by the body from FW–H equation based on the acoustic analogy theory and the research work in reference [11,12]. By normalizing the variables in these formulas an important scale rule of Helmholtz number and Mach number was derived. The scattering sound powers calculated from the scattering intensity on the surface and those calculated from the scattering sound pressure in far field should be equal to each other according to the energy conservation. The agreement of their calculation results illustrates the validity of the model and the numerical approach. The comparison of the scattering sound field calculated by present approach and by the analytical formula for a static sphere with the surface of finite impedance offers another reasonable check for the model and the approach. The numerical experiments demonstrate the scale rule of Helmholtz number and show the effects of Helmholtz number and movement velocity on the scattering sound field.

Although all numerical experiments shown in this paper are limited to the scattering by the sphere or ellipsoid, the present model is suitable to the body with arbitrary shape substantially and its main advantage is that the body movement effect can be taken into account, which is difficult to be carried out by other method.

This paper is organized in the following manner: Firstly, the model and the numerical method are presented and derived; secondly, the validity of this approach is analyzed from results of numerical experiments; then, the effects of Helmholtz number and Mach number are discussed; lastly, the conclusion is presented.

2. Math-physics model

It is assumed as follows: (a) Harmonic wave that comes from distant sonar is considered as a planar wave upon the body. (b) The body and the sonar are moving respectively in arbitrary direction with constant and small velocity (the Mach number less than 0.3 at least), so that the refraction effects of the boundary layer are negligible. (c) The body surface is inviscid and satisfies a local acting condition for the body with finite impedance surface or a refraction boundary condition for the body filled by another fluid respectively [16].

For the local acting surface (namely, normally reacting boundary), the sound wave is propagated effectively only in the direction perpendicular to the surface, such as for the surface of the honeycomb material. The boundary condition is described as follows:

$$z = z_n = -p_t/(v_{tn}\rho c) = -p_t/(v_t\rho c), \tag{1}$$

where p_t is the total sound pressure on the surface; v_t and v_{tn} are the particle velocity and its normal components, z and z_n are the ratios of the surface acoustical impedance and surface normal impedance to the fluid specific impedance respectively.

The second type of boundary condition is similar to the refraction occurring between fluids, which could be described by using the refraction theorem:

$$z_n = -p_t/(v_{tn}\rho c) = -p_t/(v_t\cos\theta_2\,\rho c) = z/\cos\theta_2. \tag{2}$$

In fact, there is another type of boundary that occurs for rigid elastic objects. A detailed discussion requires consideration of the propagation of both elastic shear and compression waves in the solid. It is beyond the discussion of this paper.

FW–H equation without quadruple and viscidity is used to solve an acoustical elastic coupling problem in Ref. [12]:

$$\Box^2 p = \frac{\partial}{\partial\tau}[\rho_0 V_n|\nabla f|\delta(f)] - \frac{\partial}{\partial y_i}[p|\nabla f|\delta(f)], \tag{3}$$

where $V_n = \bar{V}_n + v_n$, $\bar{V}_n$ is the normal velocity of the mean surface, v_n is the surface's normal velocity around the mean surface, f is the surface function and $f=0$ stands for the surface, $f>0$ and $f<0$ means outside and inside of surface respectively. The scattering sound field could be calculated by Farassat's integral form of Eq. (3) when the normal velocity and the total pressure on the surface are known:

$$4\pi p_s(\vec{x},t) = \int_{f=0} K_S(\vec{x},t,\vec{y},\tau)\,\mathrm{d}s + \int_{f=0} K_R(\vec{x},t,\vec{y},\tau)\,\mathrm{d}s, \tag{4}$$

where

$$K_R = \left\{\frac{\rho c v_n + p_t\cos\theta}{cr(1-\bar{M}_r)^3}\right\}_{ret}$$

$$K_S = \left\{\frac{\rho c v_n(\bar{M}_r - \bar{M}^2) + p_t[(1-\bar{M}^2)\cos\theta - (1-\bar{M}_r)\bar{M}_n]}{r^2(1-\bar{M}_r)^3}\right\}_{ret},$$

where the p_t and v_n are the total sound pressure and normal velocity on the surface; $\bar{M}$, $\bar{M}_r$, $\bar{M}_n$ are the Mach number, its projection in radiating direction and its normal component on the surface

respectively; θ is the angle between the normal and the radiating direction. The subscript "*ret*" signifies that the expression is to be evaluated at retarded time τ.

At present the model and numerical method are expanded to solve the scattering problem of underwater body with impedance surface. Herewith scattering sound field is induced by the total sound pressure and the normal velocity which are excited by the incident sound wave. The total sound pressure is the sum of the incident sound wave and the scattering sound pressure.

$$4\pi p_t(\vec{x},t)=\int_{f=0}K_S\,\mathrm{d}s+\int_{f=0}K_R\,\mathrm{d}s+4\pi p_i(\vec{x},t). \tag{5}$$

The singularity in the integral of K_S arises while the observer approaches the body surface. By using the same procedure as that used in Ref. [10] to move the singularity a equation linking p_t and v_n is obtained:

$$4\pi\left(1-\frac{1}{2\beta_n^2}\right)p_t(\vec{x},t)=-\int_{f=0}K_S\,\mathrm{d}s+\int_{f=0}K_R\,\mathrm{d}s+\frac{2\pi\rho c\bar{M}_n v_n}{\beta^2}+4\pi p_i(\vec{x},t)+o(\varepsilon), \tag{6}$$

where $\beta_n=\sqrt{1-\bar{M}_n^2}$, $\bar{M}_n$ is the normal Mach number of the mean surface. In Eq. (6) other variables are independent of time except p_t and v_n. A corresponding equation in frequency domain is obtained by Fourier transformation of Eq. (6).

$$\begin{aligned}&4\pi\left(1-\frac{1}{2\beta_n^2}\right)p_t(\vec{x},\omega)\\&\quad=\oint_{f=0}\left\{\frac{\mathrm{e}^{-\mathrm{i}\omega r/c}[\rho c v_n(\bar{M}_r-\bar{M}^2)+p_t((1-\bar{M}^2)\cos\theta-(1-\bar{M}_r)\bar{M}_n)]}{r^2(1-\bar{M}_r)^3}\right\}_{ret}\mathrm{d}s\\&\qquad+\int_{f=0}\left\{\frac{\mathrm{e}^{-\mathrm{i}\omega r/c}\mathrm{i}\omega[\rho c v_n+p_t\cos\theta]}{cr(1-M_r)^3}\right\}_{ret}\mathrm{d}s+4\pi p_i(\vec{x},\omega)+\frac{2\pi\rho c\bar{M}_n v_n}{\beta^2}+o(\varepsilon),\end{aligned} \tag{7}$$

where p_t and v_n are the components in frequency ω.

From Eq. (1) or (2), v_n is expressed as $p_t/(z_n\rho c)$, substituting it for v_n in Eq. (7) an equation governing the total pressure p_t on the surface is obtained:

$$\begin{aligned}&4\pi\left(1-\frac{1}{2\beta_n^2}\right)p_t(\vec{x},\omega)\\&\quad=\left\{\oint_{f=0}\left\{\frac{\mathrm{e}^{-\mathrm{i}r\cdot\omega/c}[(\bar{M}_r-\bar{M}^2)/z_n+(1-\bar{M}^2)\cos\theta-(1-\bar{M}_r)\bar{M}_n]p_t}{\bar{r}^2(1-\bar{M}_r)^3}\right\}_{ret}\mathrm{d}\bar{s}\right.\\&\qquad\left.+\int_{f=0}\left\{\frac{\mathrm{e}^{-\mathrm{i}r\cdot\omega/c}\mathrm{i}\omega[1/z_n+\cos\theta]p_t}{r(1-M_r)^3}\right\}_{ret}\mathrm{d}\bar{s}+\frac{2\pi\bar{M}_n p_t}{\beta^2 z_n}+4\pi pi(\vec{x},\omega)+o(\varepsilon).\right.\end{aligned} \tag{8}$$

From the Fourier transformation of Eq. (4) and the impedance boundary condition the scattering sound pressure could be calculated,

$$4\pi p_s(\vec{x},\omega) = \int_{f=0}\left\{\frac{e^{-ir\cdot\omega/c}[(\bar{M}_r-\bar{M}^2)/z_n+(1-\bar{M}^2)\cos\theta-(1-\bar{M}_r)\bar{M}_n]p_t}{\bar{r}^2(1-\bar{M}_r)^3}\right\}_{ret} d\bar{s} + \int_{f=0}\left\{\frac{e^{-ir\cdot\omega/c}i\omega[1/z_n+\cos\theta]p_t}{r(1-M_r)^3}\right\}_{ret} d\bar{s}. \quad (9)$$

In order to derive the scale rule in the following the variables are normalized by the characteristic length a and the incident pressure amplitude $|p_i|$:

$$\bar{r}=r/a,\quad \bar{x}=x/a,\ \bar{s}=s/a^2,\qquad \bar{p}_t=p_t/|p_i|,\quad \bar{p}_i=p_i/|p_i|,\quad \bar{p}_S=p_S/|p_i|. \quad (10)$$

Substitute them into Eqs. (8) and (9), get the dimensionless formulations as follows:

$$4\pi\left(1-\frac{1}{2\beta_n^2}\right)\bar{p}_t(\vec{\bar{x}},\omega) = \int_{f=0}\left\{\frac{e^{-i\bar{r}\cdot\omega a/c}[(\bar{M}_r-\bar{M}^2)/z_n+(1-\bar{M}^2)\cos\theta-(1-\bar{M}_r)\bar{M}_n]\bar{p}_t}{\bar{r}^2(1-\bar{M}_r)^3}\right\}_{ret} d\bar{s} + \int_{f=0}\left\{\frac{e^{-i\bar{r}\cdot\omega a/c}i(\omega a/c)[1/z_n+\cos\theta]\bar{p}_t}{\bar{r}(1-M_r)^3}\right\}_{ret} d\bar{s}+\frac{2\pi\bar{M}_n\bar{p}_t}{\beta^2 z_n}+4\pi\bar{p}_i(\vec{\bar{x}},\omega)+o(\varepsilon), \quad (11)$$

$$4\pi\bar{p}_s(\vec{\bar{x}},\omega) = \int_{f=0}\left\{\frac{e^{-i\bar{r}\cdot\omega a/c}[(\bar{M}_r-\bar{M}^2)/z_n+(1-\bar{M}^2)\cos\theta-(1-\bar{M}_r)\bar{M}_n]\bar{p}_t}{\bar{r}^2(1-\bar{M}_r)^3}\right\}_{ret} d\bar{s} + \int_{f=0}\left\{\frac{e^{-i\bar{r}\cdot\omega a/c}i(\omega a/c)[1/z_n+\cos\theta]\bar{p}_t}{\bar{r}(1-M_r)^3}\right\}_{ret} d\bar{s}. \quad (12)$$

The target strength TS of a body is obtained from back scattering sound pressure calculated in far field and the incident sound pressure as the following formulation:

$$TS=10\log(I_S r^2/I_i)=10\log(|P_S|^2r^2/|P_i|^2)=10\log(\bar{p}_S^2\bar{r}^2)+20\log(a), \quad (13)$$

where the unit of target size a is meter.

The above formulations illustrate that the surface sound pressure and the scattering sound field will be similar if the geometry is similar, and the impedance, Helmholtz number ($\omega a/c$) and Mach number are the same constant values respectively, it show the scaling rules for these numbers.

3. Numerical method

The discrete form of Eq. (8) is as follows:

$$\{B_{ij}(\omega, M, f)\}p_t = \{B_{vij}(\omega, M, f)\}p_t/z_n + p_{i,} \tag{14}$$

where

$$B_{ij}(\omega, M, f) = -\left\{\frac{e^{-i\omega r_{ij}/c}[(1-M^2)\cos\theta_{ij} - (1-M_{rij})M_{nj}]}{r_{ij}^2(1-M_{rij})^3}\right\}_{ret}(1-\delta_{ij})\Delta S_j - \left[\frac{e^{-i\omega r_{ij}/c} i\omega\cos\theta_{ij}}{cr_{ij}(1-M_{rij})^3}\right]\Delta S_j + 4\pi\left(1-\frac{1}{2\beta_{nj}^2}\right)\delta_{ij}, \tag{15}$$

$$B_{vij}(\omega, M, f) = -\left[\frac{e^{-i\omega r_{ij}/c}(M_{rij}-M^2)}{r_{ij}^2(1-M_{rij})^3}\right]_{ret}(1-\delta_{ij})\Delta S_j + \left[\frac{e^{-i\omega r_{ij}/c} i\omega}{cr_{ij}(1-M_{rij})^3}\right]\Delta S_j + \frac{2\pi M_{nij}}{\beta_{nj}^2}\delta_{ij}, \tag{16}$$

p_t, v_n and p_i are the total sound pressure, its normal velocity and the incident sound pressure distributed in the discrete points on the surface respectively. All of them and the elements of the matrix are complex variables.

The incident sound wave upon the target from distant sonar is approximated by the following plane wave:

$$p_i = p_0 e^{-i\vec{k}\cdot\vec{r}_c/c}, \tag{17}$$

where $\vec{r}_c$ is the position vector, $\vec{k} = (\omega/c)\hat{r}$ is the wave number vector in the radiation direction, $\hat{r} = \vec{r}/r$ is radiation unit vector of the plane wave. Symbol $\vec{r}$ stands for the vector from the sonar position at retarded time to target position at the observer time, the r is calculated as follows:

$$r = \frac{\vec{R}\cdot\vec{M}_S + \sqrt{(\vec{R}\cdot\vec{M}_S)^2 + (1-M_S^2)R^2}}{(1-M_S^2)}. \tag{18}$$

Here $\vec{R}$ is the vector from sonar to target when both at observation time, $\vec{M}_S = \vec{V}_S/c$ is the sonar Mach number.

In view of the Doppler effect, the frequency observed by the target is as follows:

$$\omega_O = \frac{1-\hat{r}\cdot\vec{V}_O/c}{1-\hat{r}\cdot\vec{V}_S/c}\omega_S, \tag{19}$$

where ω_O = observed frequency, ω_S = sonar frequency, $\vec{V}_O$ = target velocity, $\vec{V}_S$ = sonar velocity.

From Eq. (14), we get

$$p_t = [\{B_{ij}(\omega, M, f)\} - \{B_{vij}(\omega, M, f)/z_n\}]^{-1}\cdot p_i. \tag{20}$$

While $|z_n| \to \infty$, $p_t = [\{B_{ij}(\omega, M, f)\}]^{-1} \cdot p_i$, it is the governing equation for rigid body; while $|z_n| \to 0, p_t = 0, v_n = [\{B_{vij}(\omega, M, f)/z_n\}]^{-1} \cdot (-p_i)$, it is the equation for a body with pressure-release surface.

The scattering pressure can be obtained by using Eq. (9) after p_t is calculated.

4. The validity check by numerical experiment

The numerical checks consist of the conservation of the sound power scattered and the comparison of the scattering sound field calculated with the analytical results.

The scattering sound power by a static body in far field is $W_F = \int_\Sigma (p_s \cdot p_s^*)/\rho c \, \mathrm{d}s$, where Σ signifies a sphere around the body in far field; the complex scattering sound power on the surface can be calculated by $W_S = \int_{f=0} I_S \, \mathrm{d}s$, where $I_S = (p_t - p_i) \cdot (v_{tn} - v_{in})^*$ is the normal intensity on the surface due to scattering, and the real part of W_S should be equal to W_F due to the energy conservation. In Table 1 the comparison between the results calculated is listed for the scattering of 1000 Hz plane wave from an ellipsoid in size of (0.2 m, 0.2 m, 0.6 m) with varying surface impedance. The origin of reference frame (x,y,z) is set in the center of ellipsoid and the axis x,y,z are along with the ellipsoid radiuses a,b,c respectively, where $a \leqslant b \leqslant c$. The incident sound wave is along the z direction. In Table 1 a very good agreement of sound powers calculated from far field and those from body surface is shown, which illustrates the validity of the model and the numerical approach. The last two cases show the effects of surface boundary condition on the scattering sound power, the sound power produced by the refraction surface is much smaller than that produced by the local acting surface which illustrates that the boundary condition is very important to the scattering.

For the scattering of plane wave from a static sphere shown in Fig. 1 a series solution could be derived by classic theory [17]. The incident sound pressure p_i, its particle normal velocity v_{in} and the scattering sound pressure p_s, its normal velocity v_{sn} signed in this figure are expressed as follows:

$$p_i = p_A \mathrm{e}^{-\mathrm{j}\omega t} \sum_{m=0}^{\infty} (2m+1) j^m L_m(\cos\theta) j_m(kr), \tag{21}$$

Table 1
Sound power calculated on the surface and in far field

Refractive index	The ratio of surface impedance	Real part of surface sound power	Sound power in far field
	$(\infty, 0.0)$	0.135E−07	0.135E−07
	(0.0,0.0)	0.490E−06	0.489E−06
	(0.051,−1.329)	0.394E−06	0.389E−06
$\cdot\infty$	(0.127,−1.049)	0.645E−06	0.639E−06
	(0.042,−0.559)	0.215E−05	0.211E−05
	(0.116,−0.452)	0.951E−06	0.956E−06
	(0.162,0.19)	0.304E−06	0.306E−06
1.25	(0.162,0.19)	0.958E−08	0.100E−07

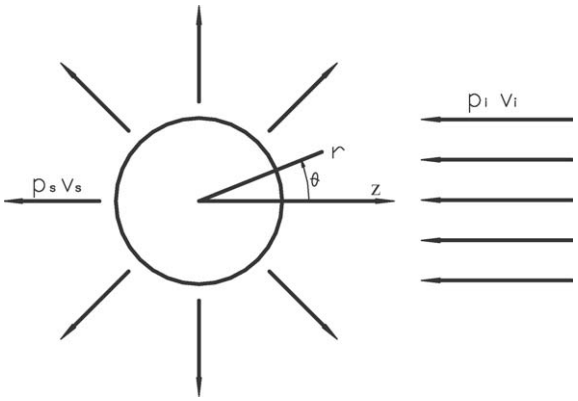

Fig. 1. Scattering of planar sound wave by a sphere.

Table 2
Parameters in numerical experiment to check present approach by comparison the results with the series solution

Situation	Incident wave frequency (Hz)	Scales of the target (m)	The ration of surface impedance	Helmholtz number
1	477.46	1.00	(∞,0.0)	2.00
2	477.46	1.00	(0.0,0.0)	2.00
3	477.46	1.00	(0.051,−1.329)	2.00
4	477.46	1.00	(0.162,0.19)	2.00
5	100.0	1.00	(0.051,−1.329)	0.42
6	100.0	1.00	(0.162,0.19)	0.42

$$v_{in} = \frac{p_A e^{-j\omega t}}{\rho_0 c_0} \sum_{m=0}^{\infty} j^{m+1}(2m+1) L_m(\cos\theta) D_m(kr) \sin\delta_m(kr), \tag{22}$$

$$p_s = \sum_{m=0}^{\infty} B_m \cdot L_m(\cos\theta) \cdot h_m^{(1)}(kr) \cdot e^{-j\omega t}, \tag{23}$$

$$v_{sn} = \frac{e^{-j\omega t}}{\rho_0 c_0} \sum_{m=0}^{\infty} B_m L_m(\cos\theta) D_m(kr) e^{j\delta_m(kr)}. \tag{24}$$

For the local acting surface condition from (1), $(p_i + p_s) = -z(v_i + v_s)\rho c,$, the B_m could be obtained as follows:

$$B_m = \frac{p_A(2m+1)j^m j_m(ka) + p_A z \cdot \rho c \cdot j^{m+1}(2m+1) D_m(ka) \sin\delta_m(ka)}{-z \cdot \rho c \cdot D_m(ka) e^{-j\delta_m(ka)} - h_m^{(1)}(ka)}. \tag{25}$$

The parameters of numerical experiments are listed in Table 2 where the incident frequencies are 477 and 100 Hz in the first four cases and the last two cases respectively.

The sound pressure contours obtained from the two approaches are shown in Figs. 2–7 where the scale is in meter. For the convenience of comparison, due to the symmetries of sound field the

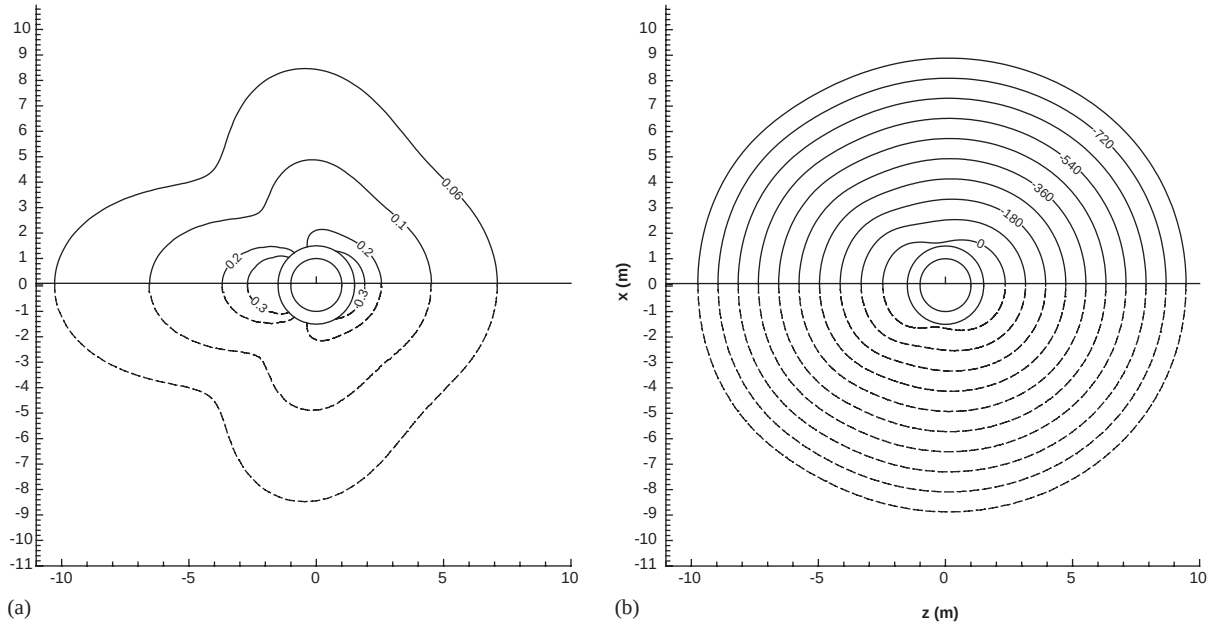

Fig. 2. Comparison of the numerical result of the present approach with that of the series solution for a sphere. Situation 1 in Table 2; incident wave frequency 477.46 Hz; radius of sphere 1.0 m; ratio of surface impedance: (∞,0.0). Comparison of the (a) amplitude contour; (b) phase contour.

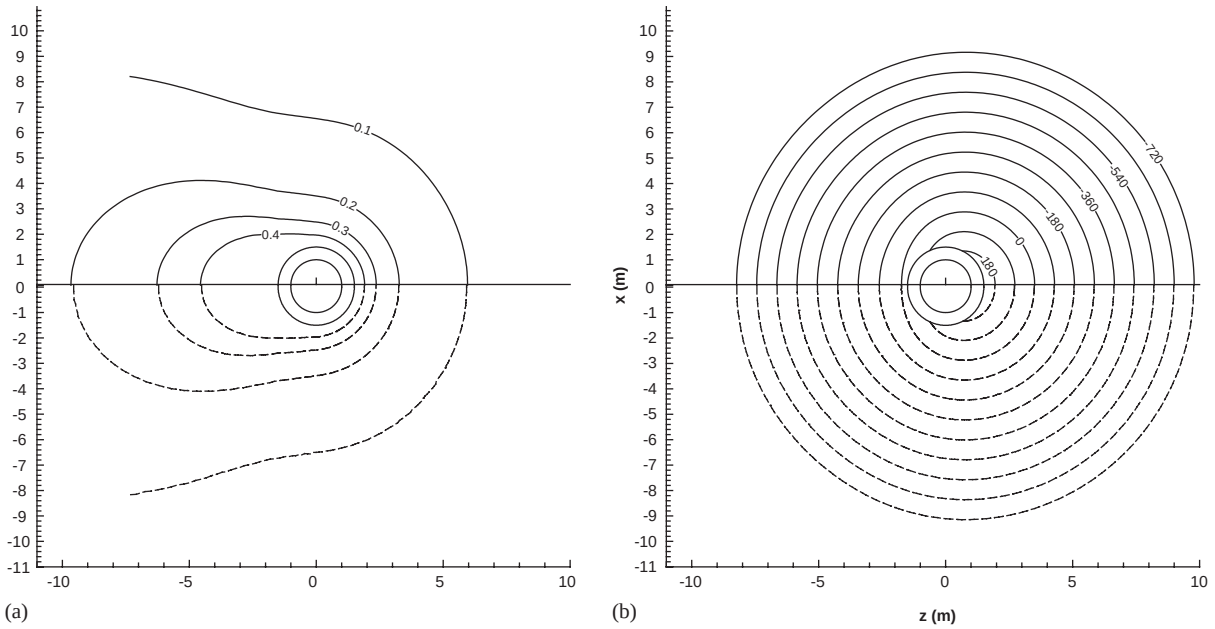

Fig. 3. Comparison of the numerical result of the present approach with that of the series solution for a sphere. Situation 2 in Table 2; incident wave frequency 477.46 Hz; radius of sphere 1.0 m; ratio of surface impedance: (0.0,0.0). Comparison of the (a) amplitude contour; (b) phase contour.

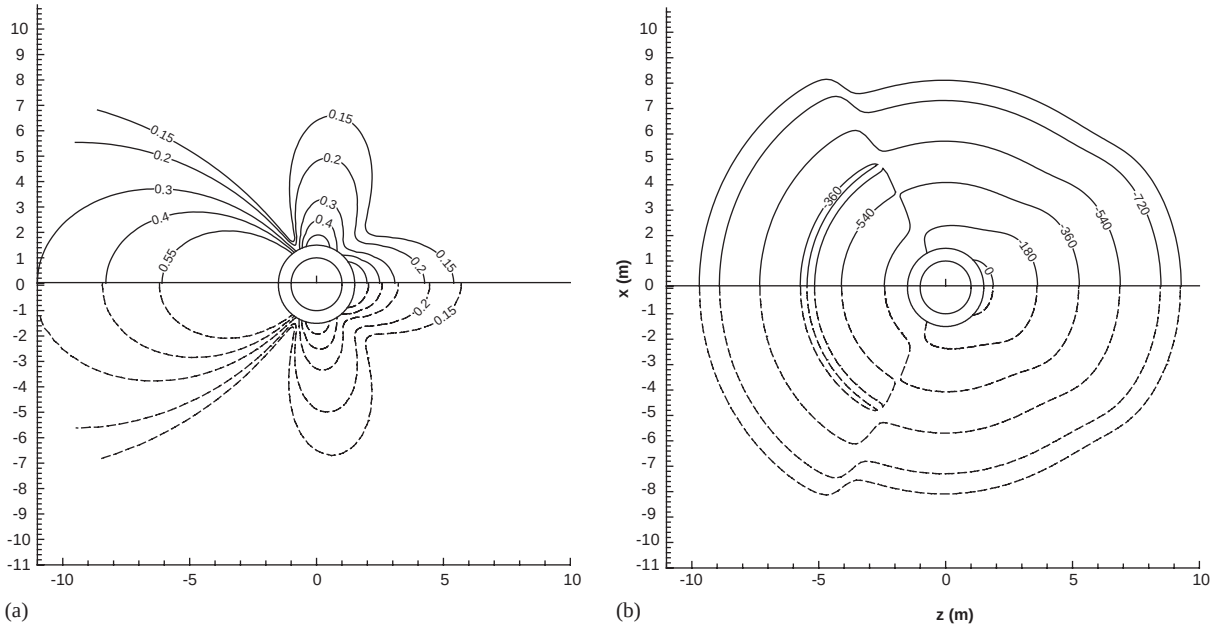

Fig. 4. Comparison of the numerical result of the present approach with that of the series solution for a sphere. Situation 3 in Table 2; incident wave frequency 477.46 Hz; radius of sphere 1.0 m; ratio of surface impedance: (0.051,−1.329). Comparison of the (a) amplitude contour; (b) phase contour.

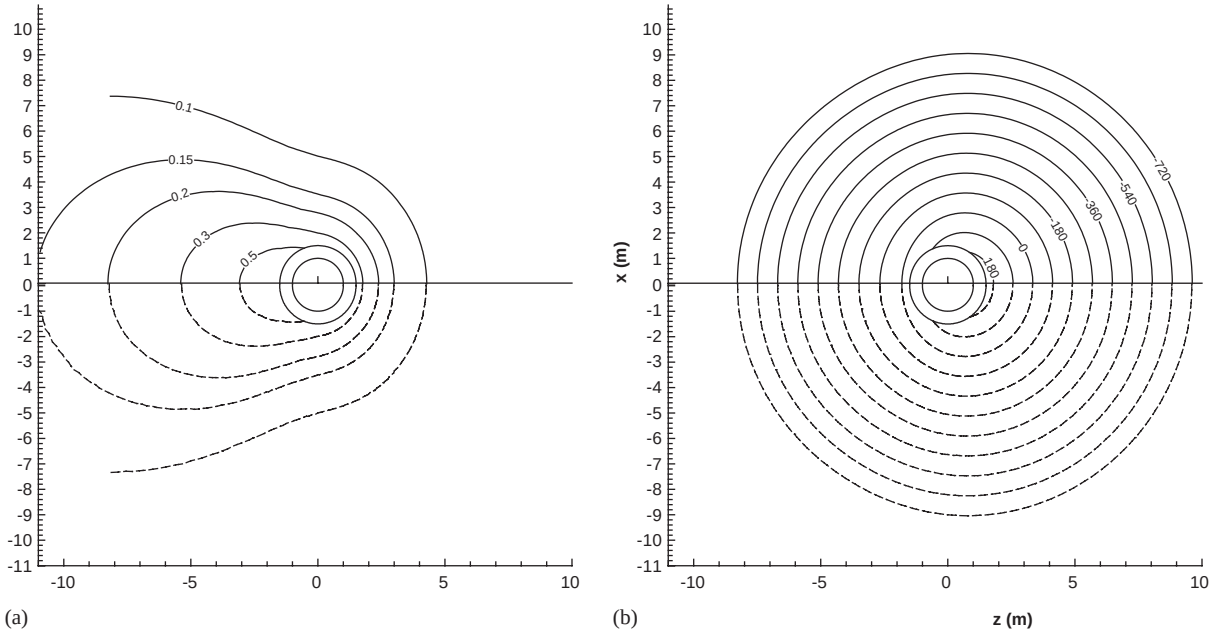

Fig. 5. Comparison of the numerical result of the present approach with that of the series solution for a sphere. Situation 4 in Table 2; incident wave frequency 477.46 Hz; radius of sphere 1.0 m; ratio of surface impedance:(0.162,0.19). Comparison of the (a) amplitude contour; (b) phase contour.

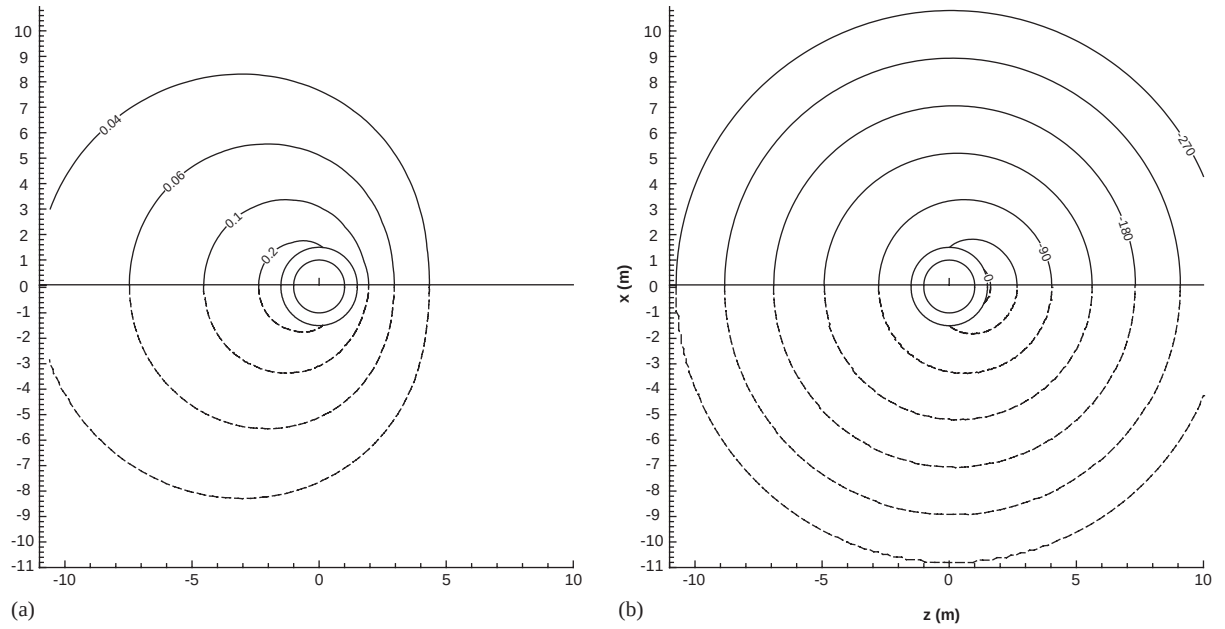

Fig. 6. Comparison of the numerical result of the present approach with that of the series solution for a sphere. Situation 5 in Table 2; incident wave frequency 100.0 Hz; radius of sphere 1.0 m; ratio of surface impedance: (0.051, −1.329). Comparison of the (a) amplitude contour; (b) phase contour.

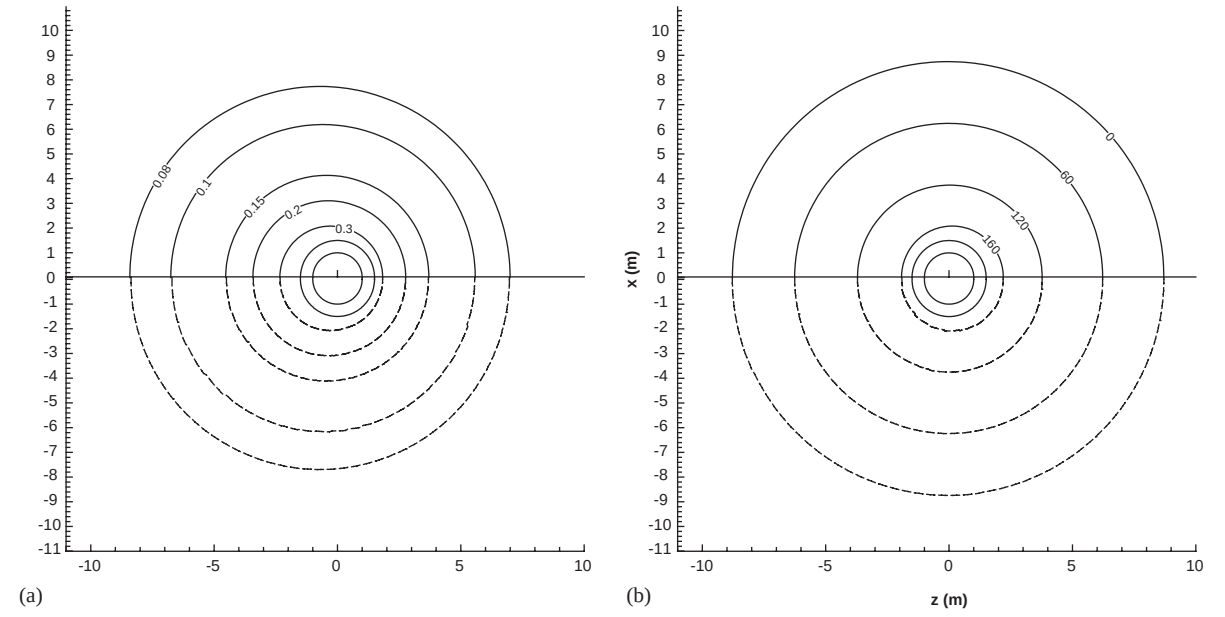

Fig. 7. Comparison of the numerical result of the present approach with that of the series solution for a sphere. Situation 6 in Table 2; incident wave frequency 100.0 Hz; the radius of sphere 1.0 m; ratio of surface impedance: (0.162,0.19). Comparison of the (a) amplitude contour; (b) phase contour.

series results are drawn in the downside with dash lines and present numerical results in the upside with solid lines respectively. The figure (a) shows the sound pressure amplitude contour and the figure (b) shows the phase contour. The region calculated to compare is out of 1.5 radius of sphere.

It is known that the phase difference between the 0° and the 360° is not a real discontinuity of phase physically. In order to eliminate this type of discontinuity, the phase values were taken in a region larger than 0°–360° in the phase contours.

In the figures, most cases show very good coincidences between the upside contours and the downside ones except in Fig. 4 where a small difference less than 12% between the upside and the downside contours was discovered, which may be due to the higher frequency and the higher acoustic reactance which cause more numerical error.

The comparison of the two results offers an evidence for the validity of present approach. From the figures the effects of boundary condition on the scattering sound field are shown very clear also.

5. The Helmholtz number effects on the scattering

In Section 2, a Helmholtz number and Mach number scale rule was derived in Eqs. (11)–(13), herewith the Helmholtz number scale rule will be demonstrated by the numerical experiments, and the results of scattering sound field for different Helmholtz number will show its effects also.

The parameters in the numerical experiments are listed in Table 3 where the cases 1, 2 and 3 are for the scattering of incident planar wave by spheres and cases 4, 5 and 6 are for the scattering of wave along with the longitudinal axis by ellipsoids. The incident wave points to the negative direction of z. The scattering sound pressure contours are shown in Figs. 8–13 (corresponding to cases 1–6 respectively), where the figure (a) is for the amplitude contour and the figure (b) for the phase contour.

In Cases 1 and 2, the frequencies of incident wave and the sizes of sphere target are different respectively, but the values of Helmholtz number are the same. That is to say there is no difference between their relative wavelengths in the two cases. From the corresponding Fig. 8 and 9, it is easy to see the complete coincidence of scattering sound field in the scaling position. And in case 3, the distribution of scattering field is greatly different from the above two due to its increased Helmholtz number which show in Fig. 10. Similarly, in case 4, 5, 6 (corresponding to Figs. 11–13

Table 3
Parameters in numerical experiment to show the effects of Helmholtz number

Situation	Incident wave frequency (Hz)	Shape	Scales of the target (m)	The ratio of surface impedance	Helmholtz number
1	100	Sphere	1	(0.0,0.0)	0.42
2	1000		0.1		0.42
3	2000		1		8.4
4	200	Ellipsoid	$1 \times 1 \times 3$	(0.162,0.19)	0.84
5	400		$0.5 \times 0.5 \times 1.5$		0.84
6	400		$1 \times 1 \times 3$		1.68

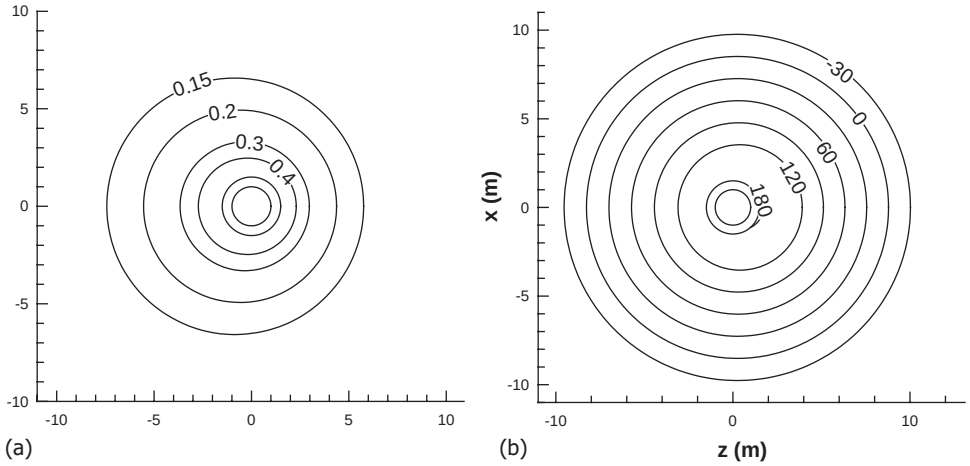

Fig. 8. Helmholtz number effect on scattering of spheres. Situation 1 in Table 3; incident wave frequency 100.0 Hz; radius of sphere 1.0 m; Helmholtz number 0.42; ratio of surface impedance: (0.0,0.0). (a) Amplitude contour; (b) phase contour.

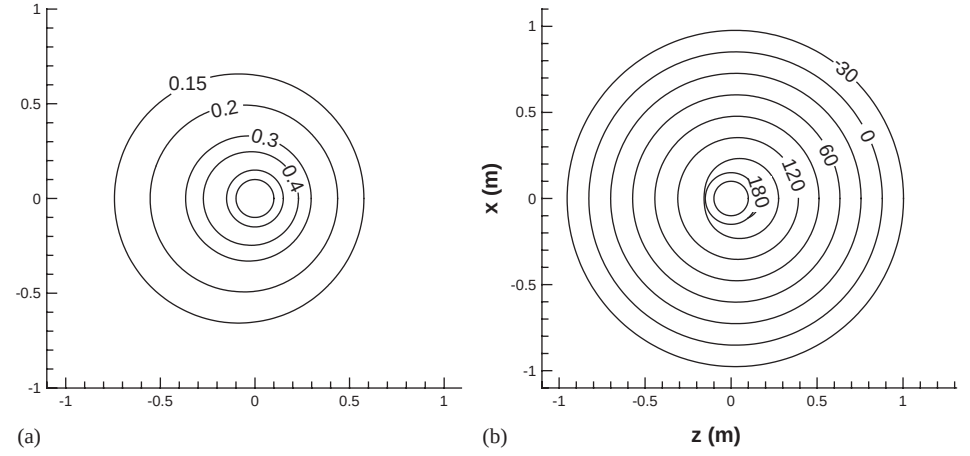

Fig. 9. The Helmholtz number effect on scattering of spheres. Situation 2 in Table 3; incident wave frequency 1000.0 Hz; radius of sphere 0.1 m; Helmholtz number 0.42; ratio of surface impedance: (0.0,0.0). (a) Amplitude contour; (b) phase contour.

respectively), the target is ellipsoid, we also observe the same result, where in the first two cases the counters are similar due to the same Helmholtz numbers, the last one is different due to the Helmholtz numbers changed. Besides, cases 1–6 also show that with the increase of Helmholtz number, more changes of scattering field distributed around the object appear. All of these display an exact scale rule of Helmholtz number and the effects of Helmholtz number on the scattering.

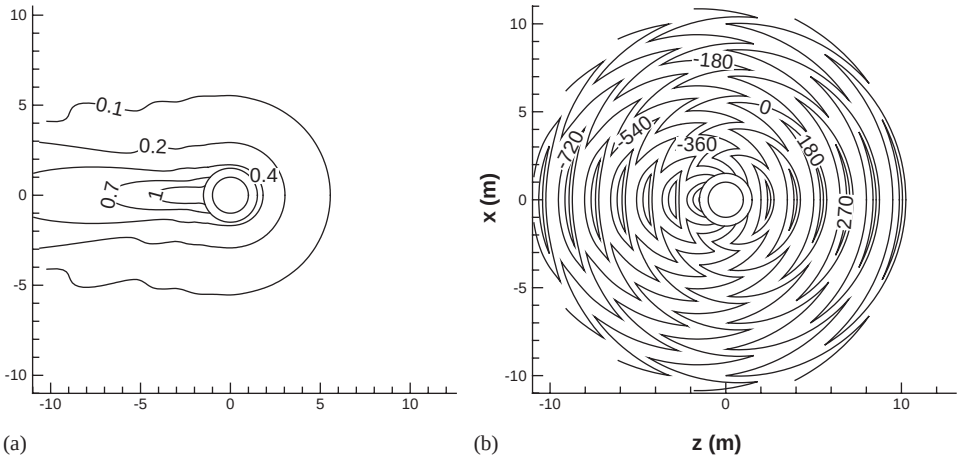

Fig. 10. Helmholtz number effect on scattering of spheres. Situation 3 in Table 3; incident wave frequency 2000.0 Hz; radius of sphere 1.0 m; Helmholtz number 8.4; ratio of surface impedance:(0.0,0.0). (a) Amplitude contour; (b) phase contour.

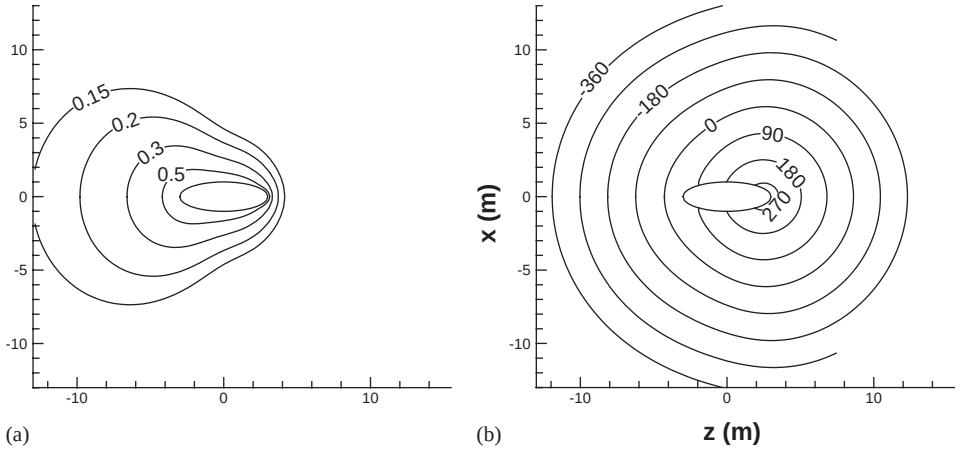

Fig. 11. Helmholtz number effect on scattering of ellipsoids. Situation 4 in Table 3; incident wave frequency 200.0 Hz; size of ellipsoid $1 \times 1 \times 3$(m); Helmholtz number 0.84; ratio of surface impedance: (0.162,0.19). (a) Amplitude contour; (b) phase contour.

6. The effect of moving velocity on the target strength

The present model and approach could account for the effects of the sonar and the body velocity efficiently as mentioned in Section 2. Herewith the cases of the ellipsoid in size (1 m, 1 m, 3 m) with surface impedance ratio of (0.051, −1.329) in the incident wave of 800 and 400 Hz are used to demonstrate the movement velocity effects on the target strength. The choice of these cases is for the convenience of discussion. Fig. 14 (corresponding to the incident wave of 800 Hz) and 15 (corresponding to the incident wave of 400 Hz) show the comparison of the target strength distribution for the static situation in solid line with the moving situation in broken line. In these

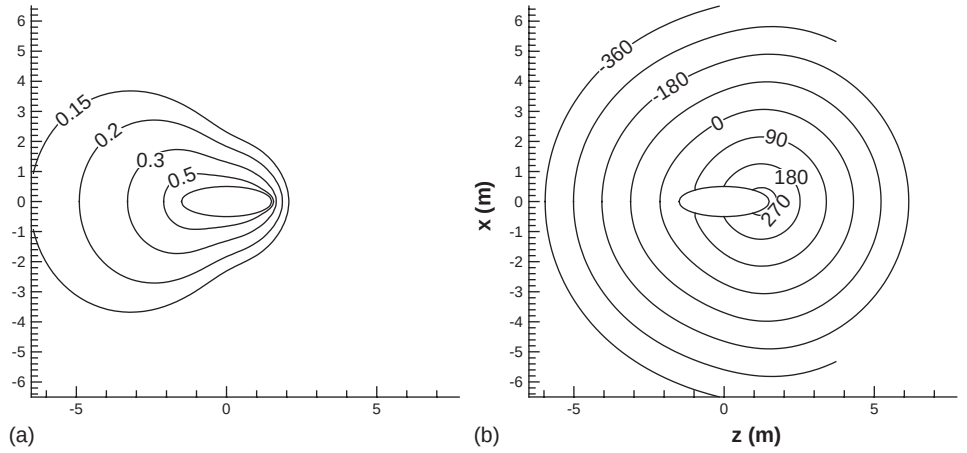

Fig. 12. Helmholtz number effect on scattering of ellipsoids. Situation 5 in Table 3; incident wave frequency 400.0 Hz; size of ellipsoid $0.5 \times 0.5 \times 1.5$(m); Helmholtz number 0.84; ratio of surface impedance: (0.162,0.19). (a) Amplitude contour; (b) phase contour.

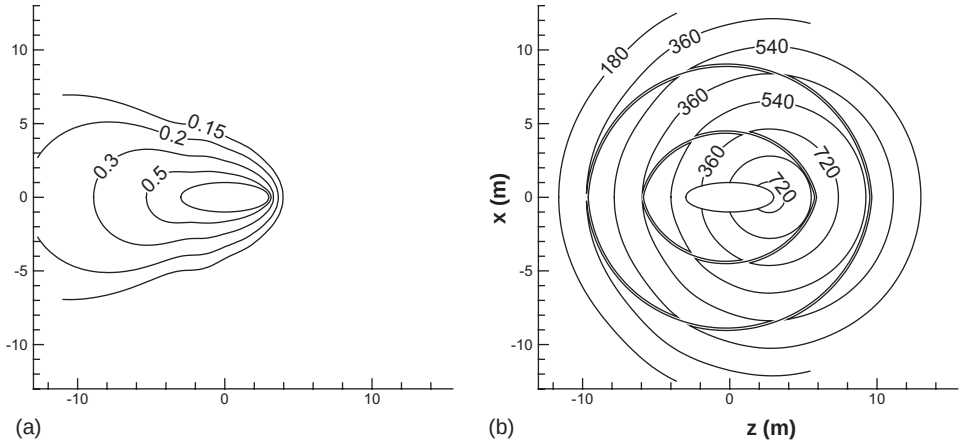

Fig. 13. Helmholtz number effect on scattering of ellipsoids. Situation 6 in Table 3; incident wave frequency 400 Hz; size of ellipsoid $1 \times 1 \times 3$ (m); Helmholtz number 1.68; ratio of surface impedance: (0.162,0.19). (a) Amplitude contour;(b) phase contour.

two cases, target velocity is (0.0, 0.0, 5.54) m/s and the sonar velocity is (0.0, 0.0, -5.54) m/s respectively, which means the target and sonar move in the opposite direction with the same velocity amplitude. These two figures show the distribution of the target strength in xz plane where the sonar direction angle begins from axis z. When moving velocity is zero (corresponding to the solid in Figs. 14 and 15), the two parts of left and right are symmetrical; when moving velocity is not zero (corresponding to the broken in Figs. 14 and 15), on the right half of the figure the target and the sonar will move closely and on the left they will move away from each other. From the Figs. 14 and 15 it can be found that due to the movement velocity on the left part the TS values will reduce and on the right part, the TS values will increase. It can be also found that the effect is more obvious in higher Helmholtz number condition (corresponding to Fig. 14) than in

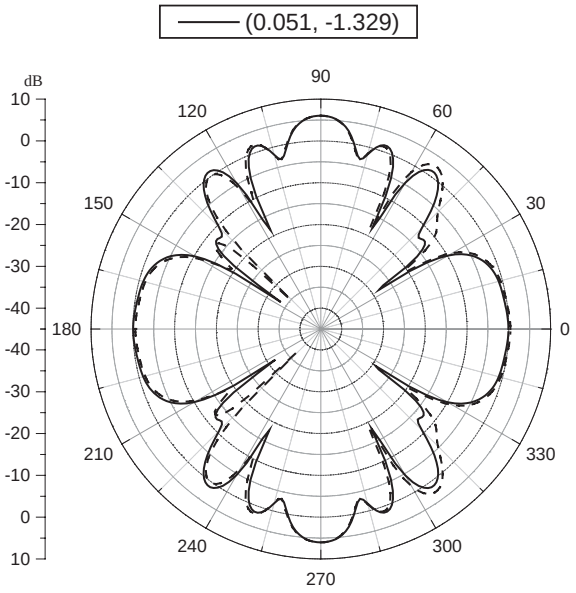

Fig. 14. Comparison of target strength distribution of the ellipsoid. Solid line: target velocity (0, 0, 0) m/s; Sonar velocity (0, 0, 0) m/s; Broken line: target velocity (0, 0, 5.54) m/s; Sonar velocity (0, 0, −5.54) m/s. Incident wave frequency: 800 Hz; size of ellipsoid $1 \times 1 \times 3$(m); ratio of surface impedance: (0.051, −1.329).

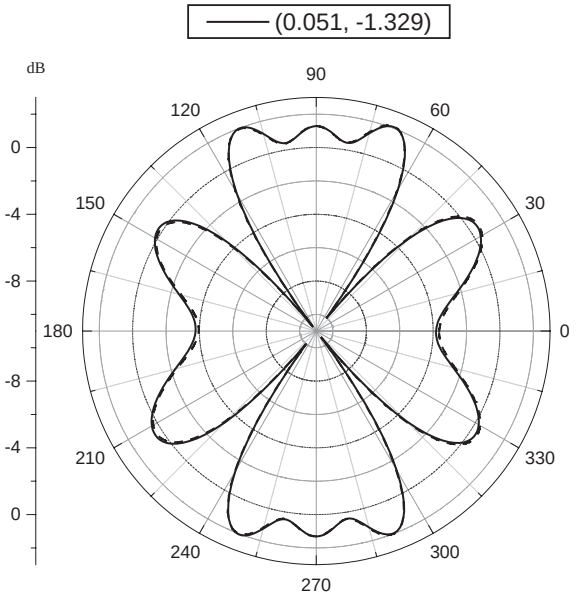

Fig. 15. Comparison of target strength distribution of the ellipsoid. Solid line: target velocity (0, 0, 0) m/s; Sonar velocity (0, 0, 0) m/s. Broken line: target velocity (0, 0, 5.54) m/s; Sonar velocity (0, 0, −5.54) m/s. Incident wave frequency: 400 Hz; size of ellipsoid $1 \times 1 \times 3$(m); ratio of surface impedance: (0.051, −1.329).

lower one (corresponding to Fig. 15). In addition, with the increase of moving velocity, the effect will be more significant.

7. Conclusion

The Lighthill's acoustic analogy theory has been successfully applied to calculate the sound scattering of plane wave by a moving body with the surface of finite impedance that is a representative boundary in engineering application. The following are concluded:

1. The agreement of the sound scattering powers calculated on the surface and in far field as well as the comparison of the scattering sound field from static sphere calculated by present approach and by analytic formula confirms the validity of the model and numerical approach.
2. The similarity of Helmholtz number and Mach number was derived and confirmed by the case of sphere and ellipsoid. For higher Helmholtz number the pressure contour of the acoustic scattering field by a sphere will be changed more severely around the sphere. The movement velocity, etc. Mach number (not zero) will cause the change of target strength distribution.
3. The different boundary condition for the body was investigated by numerical experiments, which have different acoustical energy absorption and scattering sound field. The boundary similar to the interface of different fluid causes a much smaller amount of acoustic energy absorption than that with finite impedance.
4. The present model is suitable to study the scattering by any arbitrarily shaped body moving in a small constant velocity substantially.

Acknowledgements

This work was funded by China Defense Scientific Funds (No. 98J10.5.4.HK01); this contribution is greatly appreciated.

Appendix A. Nomenclature

c	sound velocity
TS	target strength
$D_l()$	$\frac{\mathrm{d}}{\mathrm{d}z}[j_l(z) - jn_l(z)] = -jD_l(z)\mathrm{e}^{-\mathrm{j}\delta_l(z)}$
$j_l()$	l order spherical Bessel function
$N_l()$	l order spherical Neumann function
$\delta_l()$	phase shift of sphere scattering
$H_l^{(1)}()$	l order spherical Hankel function of the first kind
$L_l()$	l order Legendre function
$K=\omega/c$	wave number

K_R	regular kernel
K_S	singular kernel
$M = V/c$	Mach number
$M_n = V_n/c$	Mach number in normal direction
$M_r = V_r/c$	Mach number in propagation direction
p_A	sound pressure amplitude
p_i	incident sound pressure
p_s	scattering sound pressure
p_t	total sound pressure
v_i	velocity of incident wave
v_{in}	normal component of v_i on the body surface
v_{sn}	normal velocity of scattering wave
v_{tn}	normal component of total sound velocity on the body surface
$\vec{r} = \vec{x}(t) - \vec{y}(\tau)$	radiation vector from source to observer
$r = \lvert\vec{r}\rvert$	distance between source and observer
$\hat{r} = \vec{r}/r$	unit radiation vector
t	observer time
$\vec{V}_O$	object velocity
$\vec{V}_S$	sonar velocity,
V_n	normal velocity of the surface
$\bar{V}_n$	normal velocity of the mean surface
v_n	surface's normal velocity around the mean surface
W_F	scattering sound power calculated in far field
$\vec{x}$	observer position in frame moving
$\vec{y}$	source position in frame moving
z	ratio of surface impedance
z_n	ratio of surface normal impedance
$\beta = \sqrt{1 - M^2}$	
$\beta_n = \sqrt{1 - M_n^2}$	
$\delta(f)$	Dirac delta function
ε	size of small square hole removed from integral
ρ	density of the undisturbed medium
τ	retarded time (i.e., time of emission)
ω	angular frequency
ω_O	observed frequency
ω_S	sonar frequency
θ_2	angle of refraction
$\oint$	integration with a specific hole removed from region of integration

Subscript

Ret	expression is evaluated at retarded time

Superscript

-	symbol of normalized parameter

References

[1] C. Partridge, Acoustic scattering from viscoelastically coated bodies, *Journal of the Acoustical Society of America* 99 (1) (1996) 72–76.
[2] T.K. Stanton, Sound scattering by cylinders of finite length, III. Deformed cylinders, *Journal of the Acoustical Society of America* 86 (2) (1989) 691–705.
[3] A.A. Ferri, J.H. Girisberg, P.H. Rogers, Scattering of plane waves from submerged objects with partially coated surfaces, *Journal of the Acoustical Society of America* 92 (3) (1992) 1721–1726.
[4] J.A. Eaton, A. Regan, Application of finite element method to acoustic scattering problem, *American Institute of Aeronautics and Astronautics Journal* 34 (1) (1996) 29–34.
[5] J.P. Coyette, O. Bjorndahl, A refined boundary element/finite element technique for modeling acoustic radiation from submerged structures, *European Conference on Underwater Acoustics*, 1992, pp. 369–372.
[6] J.P. Coyette, O. von Estorff, Evaluation of finite element and boundary element technique for exterior elastic-acoustic problem, *European Conference on Underwater Acoustics*, 1992, pp. 373–376.
[7] J.E. Ffowcs, Williams, D.L. Hawkings, Sound generation by turbulence and surface in arbitrary motion, *Philosophical Transactions of the Royal Society* 264A (1969) 321–341.
[8] F. Farassat, Theory of noise generation from moving bodies with an application to helicopter rotor, NASA TR-451, 1975.
[9] F. Farassat, The united acoustic and aerodynamic prediction theory of advanced propellers in the time domain, AIAA-84-2303, 1984.
[10] L.N. Long, The compressible aerodynamics of rotating blade based on acoustic formulation, NASA TP-2197, 1983.
[11] T.Q. Wang, S. Zhou, Investigation on sound field model of propeller aircraft—the effects of rigid fuselage boundary, *Journal of Sound and Vibration* 209 (2) (1998) 299–316.
[12] T.Q. Wang, S. Zhou, Investigation on sound field model of propeller aircraft—the effects of vibrating fuselage boundary, *Journal of Sound and Vibration* 209 (2) (1998) 317–328.
[13] Wang Tongqing, Zhou Sheng, Solution of a sound field generated by the vibrating surface of a body moving at small Mach number, *Chinese Science Bulletin* 43 (1) (1998) 75–78.
[14] Xiao Yi-yong, Wang Tong-qing, Study on wing shielding effect of propeller aircraft, *Chinese Journal of Aerodynamics* 13 (3) (2000) 134–137.
[15] Wang TongQing, M. Amjad, Prediction of underwater target strength, *Chinese Journal of Acoustics* 20(1) (2001) 44–51.
[16] L.E. Kinsler, A.R. Frey, A.B. Coppens, J.V. Sanders, *Fundamentals of Acoustics*, Wiley, New York, 1982.
[17] P.M. Morse, K.V. Ingard, *Theoretical Acoustics*, McGraw-Hill, New York, 1968.